MICROENDOSCOPIC CALCIUM IMAGING IN SUPPLEMENTARY MOTOR AREA AND PRIMARY MOTOR CORTEX OF RHESUS MACAQUES AT REST AND DURING ARM MOVEMENT

Anne-Caroline Martel[*1,2,6], Damien Pittard*[1,2,6], Annaelle Devergnas[1,3,6], Benjamin Risk[2,4,6], Jonathan Nassi[5,6], Waylin Yu[5], Joshua Downer[5], Thomas Wichmann[1,2,3,6], Adriana Galvan[1,2,3,6]

(*both authors contributed equally to this work)

[1]Emory National Primate Research Center, [2]Udall Center of Excellence for Parkinson's Disease Research, [3]Dept of Neurology (School of Medicine), [4]Dept of Biostatistics & Bioinformatics (Rollins School of Public Health), Emory University, Atlanta, GA, USA
[5]Inscopix Inc., Mountain View, CA, USA
[6]Aligning Science Across Parkinson's (ASAP) Collaborative Research Network, Chevy Chase, MD, 20815

Corresponding author: Anne-Caroline Martel, amarte4@emory.edu

HIGHLIGHTS

- We used one-photon miniature microscopes and microendoscopic calcium imaging to study the activity of cortical projection neurons in supplementary motor area (SMA) and primary motor region (M1) of rhesus macaques at rest and during a simple arm reaching task.
- In a proportion of cells in SMA and M1, the calcium transients were related to arm reaches and showed directional tuning.
- Coactivity between subsets of cell pairs in SMA and M1 were found during both rest and the reaching task. The strength of coactivity was not related to the distance between cells.
- Single cell calcium transients in SMA and M1 occur in precise time sequences. The neuronal ensembles participating in the sequences (and the sequences themselves) are dynamic.

ABSTRACT

The motor cortical regions have undergone evolutionary expansion and specialization from rodents to primates. Therefore, the study of these regions in non-human primates (NHPs) is relevant to understand motor control in healthy conditions or in NHP models of movement disorders. The use of calcium imaging and miniature microscopes allows the study of multiple individual neurons in cortical regions. We used this method to examine the activities of supplementary motor area (SMA) and primary motor region (M1) in four rhesus macaques. We implanted gradient index (GRIN) lenses and expressed GCaMP6f in cortical projection neurons in these regions and imaged calcium transients for weeks to months while the animals were at rest (spontaneous or idle condition) or engaged in a simple arm reaching task. We found that in a proportion of cells, in both cortical regions, the calcium activity was directionally tuned during the arm reaching task, in agreement with previous electrophysiological findings. We identified pairs of cells, scattered across the imaging fields in SMA and M1, with synchronous activity. Finally, we found that neurons in SMA and M1 have calcium transients that occur in precisely timed sequences, and that the sequences and neuronal ensembles participating in the sequences are dynamic. The microendoscopic calcium imaging technique can be used to examine calcium dynamics in groups of corticofugal neurons in SMA and M1 and compare patterns of activity among cells.

INTRODUCTION

Non-human primates (NHPs) remain the most relevant animal models to understand human neurodegenerative diseases and design novel treatments for these conditions (Tarantal et al., 2022; Yost et al., 2023). This applies especially to cortical motor regions, as these areas have undergone significant evolutionary expansion, specialization, and re-organization (Strick et al., 2021), making NHPs the most appropriate model system for invasive studies of normal motor control, or the pathophysiology of movement disorders such as Parkinson's disease.

In primates, motor cortices include primary motor cortex (M1) and the supplementary motor area (SMA) (Nachev et al., 2008; Picard and Strick, 1996), which are components of larger frontal network structures that also involve portions of the basal ganglia and the ventral anterior and ventral lateral thalamus (Alexander and Crutcher, 1990; McFarland and Haber, 2001; Middleton and Strick, 2000). Both regions are involved in movement planning and execution, with differential responses depending on task conditions. Electrophysiological studies in behaving macaques show that the neuronal responses of M1 and SMA are similar in simple tasks, but in complex tasks, M1 activity is related to execution, while SMA activity is related to the context and sensory cues (Tanji and Mushiake, 1996).

Most studies of single cortical neurons in awake NHPs have used extracellular electrophysiological recordings. More recently, genetically-encoded calcium sensors and one-photon fluorescent miniature microscopes (miniscopes) have been used to image calcium transients in individual cells in the premotor and visual cortices in macaques (Bollimunta et al., 2021; Oguchi et al., 2021). When combined with microendoscopic gradient index (GRIN) lenses, miniscopes enable optical access to non-superficial imaging regions, and allow prolonged monitoring of multiple individual neurons in the brain region of interest. The calcium activities of identified neurons can be followed for many minutes (>20 min, typically), enabling tracking of the same cells across behavioral conditions (e.g., from rest to active movement). Furthermore, calcium sensors can be specified to a particular cellular subtype by genetically directing the expression of the sensor to a selective cell population.

The aim of this study was to examine the activity of neuronal ensembles in SMA and M1 in rhesus macaques while the monkeys were at rest (spontaneous or idle condition), and when they carried out simple arm reaches (task condition) using microendoscopic calcium imaging. We expressed the genetically encoded calcium indicator GCaMP6f in projection neurons of deep cortical layers of SMA and M1 in four subjects. We tracked the activity of the same SMA and M1 neurons across conditions, examined cell pairs for synchronous activity or inactivity, and assessed whether SMA and M1 neuronal activation followed specific sequential activation patterns. Our results lay the foundation for future studies on changes in SMA and M1 activity during the onset and development of parkinsonism and other movement related disorders in NHPs.

METHODS

The key resources used in this study (including plasmids, viral vectors, and antibodies) are listed in table 1.

Animals

Four rhesus macaque monkeys (Macaca mulatta) were used for the reported results (monkeys F, Q, U, and V, 2 males, 2 females). The animals were 4- 5 years old and weighed 5.5 - 6.8 kg at the beginning of the study. The monkeys were pair-housed in adjoining cages located in a temperature-controlled room in which they were exposed to a 12-hour light cycle, fed a standard primate diet twice daily with additional fruit and vegetable supplements, and had access to water ad libitum. All procedures were approved by the Institutional Animal Care and Use Committee (IACUC) of Emory University and were performed according to the Guide for the Care and Use of Laboratory Animals and the U.S. Public Health Service Policy on the Humane Care and Use of Laboratory Animals.

Behavioral task

Two of the monkeys (Q and U) were trained in an arm reaching task (NIMH, MonkeyLogic v2.2) while head fixed with a thermoplastic molded helmet (CIVCO medical solutions) (Drucker et al., 2015) or a surgically implanted head post. The monkeys were facing a 17-inch display touchscreen (GVision) during task performance. Training began 2-4 weeks before lens implant surgery (see below), proceeded ~1 week after the surgery, and continued until the animals reached criteria (see below).

Monkey Q was trained in a one-target task that required touching a circle (~93 mm diameter) on the display screen to receive a juice reward. For each trial, the target would randomly appear on the right, left, or center panel of the touchscreen and remained for 3 seconds (s) (unsuccessful trials), or until the monkey

touched it (successful trials), and received a drop of juice. A new trial started after a period of random duration (2-3 s), following the release of the monkey's hand from the touchscreen.

Monkey U was trained in a two-target task, in which the monkey had to touch a center target (circle, ~93 mm diameter) within 1 second, and then hold it for 0.1 s, until the appearance of a target on the left or right side of the screen (randomly presented). Once the side target appeared, the monkey had to release the target center within 1 s and touch the side target (successful trial), to receive a drop of juice. Monkey Q was not trained in the two-target task.

We considered monkeys proficiently trained in these tasks when they consistently completed at least 100 successful trials per session (about 10 minutes).

Surgery (virus injections and lens implant)

Monkeys were subjected to a surgical procedure to receive injection of viruses and implantation of GRIN lenses. This surgical procedure followed methods previously described (Bollimunta et al., 2021). The surgery was performed in sterile conditions. Monkeys were sedated with ketamine (10mg/kg), intubated for isoflurane anesthesia (1-3%), and placed in a stereotactic frame. Monkeys' vitals were monitored throughout the surgical procedure by institutional veterinary staff.

We performed two craniotomies, each measuring approximately 10 mm in diameter, targeting the arm regions of SMA in the left hemisphere and M1 in the right hemisphere. Following craniotomies, we made a small incision in the dura mater for virus injections and GRIN lens implants at each cortical site. A 25-ga needle attached to a Hamilton syringe, filled with the virus solution (1:1 mixture of AAV5-TRE-GCAMP6f (9.05x10e13 gc/ml) and AAV5-ThyStTA (5.13x10e13 gc/ml)), was lowered into the brain at the desired depths using a stereotaxic-mounted injection pump (Stoelting quintessential stereotaxic injector, Stoelting), followed by three minutes of wait time and then virus injections at 0.1 μl/min.

For M1 injections, we injected a total of 3 μl of virus solution (1.5 μl at two different cortical depths). For SMA injections, we injected a total of 5 – 8 μl of virus solution (1.5 -2 μl at three different depths). The needle remained at the injections site for at least 3 minutes after the final injection at each site.

After the virus injection, an epoxy-filled 18-gauge needle was lowered into the brain to make an incision path for the GRIN prism for M1 (1 mm diameter, 9 mm or 12 mm length) or flat lens for SMA (1 mm diameter, 12 mm length), pre-attached to a baseplate to dock a miniscope (ProView Integrated Probe or ProView Integrated Prism Probe; Inscopix). The baseplate-integrated GRIN lenses were lowered in the brain to target the middle of the dorsal-ventral coordinates of the virus injections. Following the lens implantation, a cranial chamber was positioned around each baseplate-integrated GRIN lens, affixed to the skull, and capped for protection throughout the duration of the study. The exposed brain tissue around the lens was covered with gel foam and a slotted aluminum disk. The implant was secured to the disk and skull within the chamber with Metabond dental cement (Parkell, Edgewood, NY) or Gradia Direct Flo light-cured composite (GC Corp., Tokyo Japan). Finally, the exposed skull was covered with bone screws and dental acrylic.

Calcium imaging data acquisition

Following 1 to 8 weeks from surgery, we began to image calcium transients in SMA and M1 neurons using a head-mounted miniscope from Inscopix (nVista3.0, Inscopix, CA, USA). The miniscope was docked to the integrated baseplate of the implanted GRIN lenses and used to enable optical access in our brain regions-

of-interest. Imaging data for each site were acquired at least twice weekly. During these sessions, the monkeys were sitting on a primate chair and remained awake (confirmed by continuous monitoring of open eyes). Head movement was restricted by a thermoplastic helmet or by a head post to facilitate miniscope docking and to keep the monkey facing the touchscreen. In each session, we performed 20 minutes of imaging in the 'spontaneous' (idle) condition during which the monkeys performed only occasional spontaneous movements of arms, trunk, and legs, followed by imaging while the animals worked on the reaching task for as long as it took to complete 100 successful trials (median 12 min, inter-quartile range (IQR) 3.5 min). The miniscope remained mounted until the end of the session. The total duration of ecording sessions was 20 to 40 min. Imaging and recording parameters were controlled using the Inscopix data acquisition software (IDAS, Inscopix), with the following range of parameters used in all recordings: frame rate, 10 Hz; LED power, 0.6-0.8; sensor gain, 7-8, and electronic focus, 400-900.

Data analysis

Cell identification and trace extraction

Raw calcium imaging recordings were imported into the Inscopix data processing software (IDPS, Inscopix) for cell identification and trace extraction. The image processing workflow began with preprocessing of the recording by cropping out excess pixels, correcting defective pixels, and performing 4x spatial down sampling of each image frame. We then applied a spatial band-pass filter (low and high cut-off points of 0.005 $pixel^{-1}$ and 0.5 $pixel^{-1}$, respectively) to enhance the visualization of the signal and performed rigid translation motion correction with a mean projection image as the global reference frame to eliminate brain movement artifacts. Following that, we used the constrained nonnegative matrix factorization for microendoscopic data (CNMFe) algorithm (Zhou et al., 2018) to extract individual cells and their corresponding calcium transients from our recordings. Using this approach, we were able to identify and accept or reject cells based on imaging metrics such as spatial footprints, cell size, and signal-to-noise ratio. Cells with abnormal shapes or calcium dynamics were rejected from further analysis. On accepted cells, we deconvolved the traces using the OASIS method to estimate the underlying neural spikes in our calcium traces. For each session, we calculated the distance between the cells based on their centroids (x and y coordinates of cell's center), using the cell maps extracted from CNMFe. These data were then extracted for further analyses in MATLAB.

Statistical comparisons of calcium activity

For each cell in the SMA and M1, we calculated calcium event rates, inter-event interval coefficient of variation (IEI CV), and the mean amplitude of events during spontaneous and/or reaching task conditions. Statistical comparisons between spontaneous and task conditions in the SMA and M1 were performed using a Wilcoxon rank sum test. For monkey U, comparisons were also performed between SMA and M1 for spontaneous and task conditions. Statistical significance was set at $p < 0.05$.

Alignment to behavioral events

For each cell, we examined the alignment of calcium activity (using raw calcium transient) to the arm-reaching task behavior. For each successful trial, the 3 s epoch of raw data starting 1 s before target appearance (for Monkey Q) or starting 1 s before second target appearance (for Monkey U) was Z-scored to the corresponding inter-trial intervals. The mean and standard deviation of these data were calculated across all trial conditions of a given cell (right, center, or left for Monkey Q and right or left for Monkey U). Comparisons were made using non-corrected paired *t*-tests on the Z-scored data and significance was set at $p < 0.05$. Cells were characterized as modulated if the mean calcium activity during the reaching movement (0-1 s after the target appeared for Monkey Q and 0-1 s after the second target appeared for Monkey U) was significantly different than the mean activity from the 1 s period preceding the target

presentation for Monkey Q and the release of the center target for Monkey U. Results from example sessions can be seen in figure 2 and figure S1.

Cell coactivation (Jaccard)

We examined the synchrony between calcium events using the Jaccard index. We analyzed one session from each site (SMA and/or M1) in each monkey corresponding to the session with the most cells identified. Following Parker et al. (2018) (Parker et al., 2018), we first binned the spike data into 0.2 s intervals, then forward smoothed that data by setting a bin equal to one if a calcium event occurred at any time during the current bin or four bins ahead (a total of one second). We then calculated the Jaccard index between all cells (the intersection of the number of forward-smoothed events divided by the union). For each cell pairing, we generated the null distribution of Jaccard indices by randomly circularly shifting the data in one of the cells and calculating the Jaccard index between the circularly shifted cell and the other cell. This was repeated 1,000 times. The circular shift preserves the autocorrelation structure of the forward smoothed event data. Next, for each cell pairing, we calculated a normalized version of the Jaccard index by subtracting the mean of the randomly shifted Jaccard indices from the observed Jaccard index and dividing by the standard deviation of the randomly shifted Jaccard indices, which we refer to as the Z-Jaccard. Large positive values of Z-Jaccard indicate cells pairs whose events co-occur substantially more than random circular shifts of the data, which is evidence of synchrony. Large negative values indicate cell pairs whose events co-occur less than expected by random circular shifts of the data. We define negative values of the Z-Jaccard as asynchrony.

We used the centroid information to examine whether there was a relationship between the Z-Jaccard and the distance between cells. A loess smoother (span=1) was used to visualize the relationship between Z-Jaccard and distance.

Determination of precise timed sequences of calcium events

Sequence detection of calcium events was performed using a custom MATLAB algorithm. Sequences are defined as the occurrence of two or more calcium events in a defined series (neuron A -> neuron B -> neuron C) among two or more cells, occurring within a specific time range between the individual events (in this case, 2s). Using the deconvolved calcium event data exported from IDPS, we evaluated sequences occurring during 10 min segments of spontaneous and arm-reaching task conditions. The algorithm searches for the occurrence rate of all possible combination of cells within a given record and identifies those as being significant if they occurred more often than in shuffled data, using 1,000 circular re-arrangements of spike trains (outside of the 95th percentile). Based on the resulting data, we evaluated the number of such sequences, the duration of sequential events among cells, the number of sequence repetitions (example depicted in Figure 4A-B), and the spatial distance of sequence members (using the centroid values, see above).

Histology

At the conclusion of the experiments, monkeys were euthanized with an overdose of pentobarbital sodium (100mg/kg, iv). Monkeys were then transcardially perfused with oxygenated Ringer's solution, followed by 2 liters of fixative [4% paraformaldehyde, 0.1% glutaraldehyde in phosphate buffer (0.1 M, pH 7.2)]. The fixed brains were then removed and blocked. The blocks were later cut into 60 µm slices using a vibratome and immunostained for the neuronal marker microtubule-associated protein 2 (MAP2) and green fluorescent protein (GFP) to examine lens placement and GCaMP6f expression in neuronal cell bodies of projection neurons, respectively. To confirm the identity of the GCaMP6f expressing neurons, we

performed double fluorescent immunolabeling for GABA (as a marker of interneurons, expecting lack of co-labeling with GFP (GCaMp6f-positive) neurons). See table 1 for antibody details.

RESULTS

We studied the neuronal activity of SMA and M1 in four macaques using one-photon miniature microscopes and microendoscopic calcium imaging. We used AAVs to express GCaMP6f under control of the Thy1 promoter to target preferentially projection neurons (Feng et al., 2000) in deep cortical layers. All four animals received GRIN lenses in SMA in the left hemisphere and M1 in the right hemisphere, however successful calcium imaging was achieved in three SMA sites (monkeys Q, U and F) and two M1 sites (monkeys V and U).

General description of calcium activity

Calcium imaging of SMA and M1 started 1-8 weeks after injection of the virus and implantation of the GRIN lenses. Head-mounted one-photon microendoscopic calcium imaging recordings were taken while the animals were sitting in the primate chair and making occasional spontaneous movements ("spontaneous" condition) or performing the reaching task ("reaching task" condition, only monkeys Q and U).

Individual cells and their calcium dynamics were identified using the CNMFe algorithm and accepted based on their activity and morphology (figure 1 A-C). Although we found GCaMP6f expressing cells in all imaging sites, the total number of cells found per site and across sessions was highly variable. In the SMA, we identified 129, 61 and 63 cells in monkeys Q, F and U, respectively, over 54 to 125 days. In M1, we identified 37 and 23 cells in monkeys U and V, respectively, over 42 days (table 2). We were not able to reliably track the same neurons across sessions. However, we followed a small proportion of identified cells through more than one recording session (18% overall). In the results, we combined all cells across sessions per imaging site and will describe their activity during their first occurrence over the recording sessions.

Calcium events were extracted from the raw calcium traces using the deconvolution method (OASIS, see Methods for details), providing an estimate of neural spiking activity underlying the calcium transient. We used the resulting data to characterize the activity of cells recorded across multiple sessions and compare the activity during spontaneous and reaching task in SMA and M1. We assessed the median event rates, inter-event interval coefficient of variation (IEI CV), and event amplitudes for each imaging site. The events rate and IEI CV did not differ between the spontaneous and reaching task condition in either cortical region (figure 1D-E), except for Monkey U, in which the EIE CV in reaching task was significantly lower than in spontaneous ($p=0.011$; Wilcoxon sum rank test). The amplitudes of the calcium events were, in most cases, significantly higher during the reaching task compared to spontaneous, in both SMA and M1 ($p<0.0001$; Wilcoxon sum rank test). Finally, the event rate in M1 was higher than in SMA, regardless of condition (based on results from monkey U, for which data was available from both structures; figure 1D-E).

Calcium activity in SMA shows movement-related and directional tuning responses

We assessed the activity of neurons in SMA and M1 response in the reaching task. The heat maps in figure 2A show the average raw calcium traces of 129 cells in Monkey Q, recorded in the SMA across 7 sessions (see Methods). By aligning the activity of the cells to the presentation of the reaching target, we found that 39% (50/129) of cells significantly modulated their activity in response to the presentation of the

reaching target (non-corrected T-test $p<0.05$). For some cells, the activity was modulated regardless of the direction of the reach (left, center or right) (22%, 11/50), but most have a response that was specific for left or right (directional tuning, 78% (39/50) of cells). This is illustrated in figure 2 B-C. For example, cell #112 displays an increased calcium activity at the presentation of the left-sided target, compared to the presentation of the target at the center or the right of the screen. On the other hand, cell #80 showed a significant increase of calcium activity to the target presentation, regardless of position.

A similar analysis was carried out for data from the SMA of Monkey U during a session in which the animal was performing the two-target reaching task. On the heatmap (figure S1A) the average raw calcium traces are aligned on the appearance of the side targets (right or left). As for Monkey Q, we found that 50% (7/14) of cells significantly modulated their activity in response to the presentation of the reaching target (non-corrected T-test $p<0.05$). Only the activity of one cell was modulated regardless of the direction of the reaching target (left or right) (14%, 1/7), while the other cells showed directional tuning of their response (86%, 6/7). In figure S1B, cell #5 shows a significant increase of calcium activity when the side target is presented on the right, but not on the left ($p=0.01$ target right, $p=0.35$ target left, T-test).

In Monkey U, we also assessed the cell activity modulation in M1 during the two-target reaching task. Figure S1C shows the average raw calcium traces of 6 cells of an example session, aligned to the presentation of the side targets (left or right). In this session, 83% (5/6) of the cells were significantly modulated in response to the presentation of the reaching target. Among them, one cell showed selectivity towards the left target (20%, 1/5) while the other cells were selectively modulated regardless of the directionality (80%, 4/5). In figure S1D, cell 1 is significantly up-modulated toward both right and left targets ($p=0.0001$ target right, $p=0.01$ target left, T-test).

Cells in SMA and M1 show coactivation

We then explored the dynamics of calcium activity at the level of the population of cells. We examined the synchrony between calcium events using the Jaccard index (see Methods). The Jaccard index provides a statistical measure of synchrony between pairs of cells. For each animal and brain region (SMA and/or M1), a session is shown in figure 3. Based on the Z-Jaccard index from the events, populations of neurons exhibited neural synchrony in the SMA during the spontaneous condition (left column, figure 3A). Some neurons also exhibited neural synchrony in M1 in the same condition (left column figure 3B). Asynchronous cells, indicated by the negative Z-Jaccard indices, were also seen in M1. The cell populations exhibiting synchrony were not related to distance in either SMA (right column figure 3A) or M1 (right column figure 3B). We also found no relationship between the unnormalized Jaccard index and distance (not shown). In the reaching task, we also found no relationship between the Jaccard index and distance.

Cells in SMA and M1 display precisely timed sequences

Beyond the synchrony between cells in a population, i.e., coincident activities of cells, we also examined if ensembles of neurons activate in precisely timed sequences. We defined a sequence as a series of calcium events involving multiple cells, occurring in a specific temporal order, during a 10-minute period of recordings in the spontaneous condition and reaching task. As shown in the example session from Monkey Q in the SMA (figure 4A), across 40 cells, we detected 13 sequences in the 'spontaneous' record and 17 sequences while the animal was carrying out the reaching task (top panels). Even though some of the sequences detected in both conditions involve the same cells (white dots on the cell map, figure 4A bottom panels), the sequences detected are different. As an example, activity in cell #5 starts sequences

(marked with green dots and arrows, bottom panels in figure 4A.) in both conditions. However, the specific sequences initiated by this cell were different in each condition.

To test whether these different sequences are the result of different conditions (spontaneous or reaching task), we performed the same analysis for sessions where we had 20 minutes of spontaneous recording, allowing us to segment the video into two periods of 10 minutes (spontaneous 1, spontaneous 2). As shown in figure 4B, across 18 cells, we detected 8 and 13 sequences in 'spontaneous 1' and 'spontaneous 2' respectively, and 9 sequences during the reaching task. We did not find any identical sequences across the 3 segments (marked with green dots and arrows, bottom panels in figure 4B). Importantly, the sequences were distinct even between the two spontaneous segments. These differences are thus unlikely to be due to a condition effect. We carried out the same analysis for all sessions in all our animals in SMA and M1 and observed the same results (data not shown).

We also investigated whether there is a spatial relationship between cells involved in the same sequence. Plotting the distribution of distances between pairs of cells that were involved in sequences, as well as the overall distribution of distribution of distances between all detected cells (figure 5A) showed that there is no preferred spatial relation between cells involved in sequences in SMA or M1.

Finally, the detected sequences were characterized by different factors: number of sequences detected, repetition rate of sequences over the 10 minutes recording, number of steps of the sequences, and proportion of cells involved in sequences. Figure 5B summarizes these parameters for each animal in SMA and M1 (medians values across all the sessions per animal). As previously discussed in the results of figure 4A, these factors do not seem to be modulated by condition (spontaneous vs. reaching task). However, for Monkey U for which we have data both in SMA and M1, for a given population of cells, we found more sequences of activation in M1 compared to SMA, along with more instances of repetition of sequences.

Expression of GCaMP6f and lens localization

At the end of the experiments, we conducted post-mortem histological studies to confirm lens and prism placement in SMA and M1 and the expression of GCaMP6f. Figure S2A illustrates the location of the lens in the SMA (orange area) of Monkey Q (green dot), Monkey F (blue dot) and Monkey U (yellow dot) and the location of the prism in M1 (blue area) for Monkey U (yellow dot) and Monkey V (red dot). The reconstruction and location of the lens/prism in the deep layers of the SMA/M1 cortex was confirmed on the MAP2 section (right panels figure S2A), along with the interaural position (according to the atlas of Paxinos et al 2000). The expression of GCaMP6f was revealed by peroxidase against GFP (figure S2B). We observed a robust GFP expression in the area around the lens/prism for all our animals (with a weaker expression in the SMA of Monkey U).

GCaMP6f expression was also confirmed by endogenous green fluorescence, as shown in the example in figure S2C, showing endogenous green fluorescence in neuronal cell bodies in the SMA of Monkey Q.

Finally, we examined the type of neurons expressing GCaMP6f. We used GABA immunohistochemistry to identify GABAergic interneurons, with the expectation that GCaMp6f-positive cells would not express GABA. In figure S2D (Monkey U, SMA), we show that neurons with morphology of pyramidal cells are GFP-positive but GABA negative. We did not find double labeling of GABA and GFP expressing cells, suggesting that GCaMP6f+ cells are likely to be projection neurons and not interneurons.

DISCUSSION

We report for the first time the use of miniscopes and calcium imaging to examine the activity of projection neurons in deep layers of SMA and M1 of four rhesus macaques, during rest (idle condition) and while performing a simple arm reaching task. In agreement with previous studies using electrophysiology, we found that a proportion of SMA and M1 neurons displayed calcium transients in relation to arm reaches, and in some cases, these were directionally tuned. This microendoscopic calcium imaging approach allowed us to identify cell pairs in SMA and M1 that show coincident activity. Interestingly, these cell pairs were not located close to each other, but rather spread out across the imaging field. Furthermore, we report that neurons in SMA and M1 have calcium transients that occur in precisely timed sequences, and that the sequences and neuronal ensembles participating in the sequences are dynamic.

Our study complements the extensive literature on the electrophysiological activity of SMA and M1 neurons in macaques (Nachev et al., 2008). The calcium imaging method offers unique opportunities to increase our understanding of cortical activity in NHPs. The GRIN lenses allowed us to image many neurons in deep layers in both M1 and SMA. Notably, in SMA we positioned the lenses along the medial wall of cortex and the lenses were inserted as deep as 6 mm in cortex. Furthermore, by combining a genetic strategy (use of the Thy1 promoter which targets preferentially projection neurons (Feng et al., 2000) and placing the GRIN lenses in deep cortical layers, we selectively monitored cortico-fugal neurons.

While previous electrophysiological studies in the monkey SMA or M1 focused on the neuronal activity during motor tasks (e.g., (Tanji and Mushiake, 1996)), we compared calcium activity from the spontaneous to the active (reaching task) condition in individually identified neurons that were reliably tracked within a session. We found that neither the rate of calcium events nor their variability (measured with IEI CV) differed significantly between the two conditions, perhaps indicating that the information coded by these parameters is not indicative of the behavioral state of the animal (but see (Kondo et al., 2018)).

We found that in a subpopulation of SMA and M1 neurons the calcium activity was related to arm reaching events, and some neurons (particularly in SMA) showed directionally tuning, as previously observed with electrophysiological recordings (Chen et al., 1991; Nachev et al., 2008; Tanji and Mushiake, 1996). Also, similar results were reported in a previous study using miniscopes and calcium imaging in the M1 of marmosets (Kondo et al., 2018). Thus, even though the time resolution of calcium transients is orders of magnitude lower than electrophysiological recordings, the calcium imaging method can detect basic functional parameters of these cortical regions.

One important advantage of microendoscopic calcium imaging is the ability to monitor many cells simultaneously in a relatively large area of cortex, allowing analysis of simultaneous and sequential activation of neurons. Both in SMA and M1 we found pairs of cells that that were coactive. However, these cell pairs were not spatially close, indicating that there could be long range connections among them, or they could be connected through multi-synaptic pathways.

Interestingly, we discovered that neurons in M1 and SMA establish precisely timed (and sometimes recurring) sequences of activity. Surprisingly, however, these sequences were dynamic (i.e., the temporal pattern and cells involved in the sequence change with time), and these variations were observed not only when the monkeys transitioned from the spontaneous to the arm reaching task, but even throughout the spontaneous condition. These sequences could perhaps be related to other functional processes not directly assessed in our study, such as attentional or motivational states. Analysis of timed sequences has

been conducted before, mostly to study patterns of discharge of single neurons (e.g., (Galvan and Wichmann, 2023; Lestienne and Strehler, 1987)). As far as we know, this is the first report of the use of calcium imaging to examine neuronal sequential activation patterns.

The calcium imaging technique has some important limitations that need to be mentioned. First, the calcium transients captured by this method provide slower kinetics than what is achievable with electrophysiological recordings. The temporal resolution could be a restriction when examining processes dependent on faster time scales. Furthermore, the rate of calcium events is analysis-dependent. For instance, in our study the rate of calcium events was about 10-fold higher than previously reported in the premotor cortex of rhesus macaques (Bollimunta et al., 2021). The rate of calcium events we detected was also different from that reported in the M1 of marmosets (Kondo et al., 2018). These discrepancies are likely not only related to species differences (in the case of the marmosets), but also a direct result of the method used to extract calcium events (e.g., we used deconvolution, while Bollimunta et al (2021) did not).

One advantage of the calcium imaging technique using miniscopes is the ability to track the same cells across days (Sheintuch et al., 2017). In our studies we were not able to consistently track the same neurons across multiple sessions. This issue was also reported in studies conducting calcium imaging in the M1 of rats (Boschen et al., 2024). Several factors may impact the ability to longitudinally track calcium transients in the same cells over weeks or months using miniscopes in chronic preparations. It is possible that the expression of GCaMp6f is unstable and decreases with time. However, based on the robust expression of the calcium sensor that we observed in the histological post-mortem analysis, this is unlikely to be the case in our studies. We suspect, however, that changes in the field of view, due to movement of the brain tissue in relation to the GRIN lenses, may have hampered tracking of the same neurons across days, and may have also caused loss of fluorescent signals in some of the imaging sites in our study.

In summary, we used microendoscopic calcium imaging to study groups of neurons in the SMA and M1 in rhesus macaques, across behavioral states. Our studies set the stage to use this method to examine neuronal (calcium) dynamics in groups of cells in motor cortices, and may be used to compare patterns of activity among cells from healthy conditions to disease states, like in NHP models of induced parkinsonism (Chocarro et al., 2023; Masilamoni and Smith, 2018), and to study neuronal responses to acute or chronic treatments in these models. Importantly, even though we were not able to track the same cells across sessions in many cases, we imaged the same field of view (and functional region) over several days and weeks. Finally, given the ongoing development of enhancer sequences that can be used in AAVs or other viral vectors (Vormstein-Schneider et al., 2020) , it may soon be possible to expand this technique to track the activity of other neuronal subtypes (e.g., subtypes of cortical inhibitory interneurons, or specific cortical projection neurons).

ACKNOWLEDGMENTS AND FUNDING SOURCES

We are grateful to Wendy Williamson Coyne for assistance during surgeries, and to Susan Jenkins, DeErra Locklin and Charlotte Armstrong for technical help. Some of the surgeries described in this study were conducted in collaboration with Emory Translational Neuroscience Core, which is supported by the Department of Neurosurgery, Emory University School of Medicine.

This research was funded by Aligning Science Across Parkinson's [ASAP-020572] through the Michael J. Fox Foundation for Parkinson's Research (MJFF).

REFERENCES

Alexander, G.E., and Crutcher, M.D. (1990). Functional architecture of basal ganglia circuits: neural substrates of parallel processing. Trends in neurosciences *13*, 266-271.

Bollimunta, A., Santacruz, S.R., Eaton, R.W., Xu, P.S., Morrison, J.H., Moxon, K.A., Carmena, J.M., and Nassi, J.J. (2021). Head-mounted microendoscopic calcium imaging in dorsal premotor cortex of behaving rhesus macaque. Cell Rep *35*, 109239.

Boschen, S.L., Seethaler, J., Wang, S., Lujan, W.D., Silvernail, J.L., Carter, R.E., Chang, S.Y., and Lujan, J.L. (2024). Midbrain dopaminergic degeneration differentially modulates primary motor cortex activity and motor behavior in hemi-parkinsonian rats. Res Sq.

Chen, D.F., Hyland, B., Maier, V., Palmeri, A., and Wiesendanger, M. (1991). Comparison of neural activity in the supplementary motor area and in the primary motor cortex in monkeys. Somatosens Mot Res *8*, 27-44.

Chocarro, J., Rico, A.J., Ariznabarreta, G., Roda, E., Honrubia, A., Collantes, M., Penuelas, I., Vazquez, A., Rodriguez-Perez, A.I., Labandeira-Garcia, J.L.*, et al.* (2023). Neuromelanin accumulation drives endogenous synucleinopathy in non-human primates. Brain.

Drucker, C.B., Carlson, M.L., Toda, K., DeWind, N.K., and Platt, M.L. (2015). Non-invasive primate head restraint using thermoplastic masks. J Neurosci Methods *253*, 90-100.

Feng, G., Mellor, R.H., Bernstein, M., Keller-Peck, C., Nguyen, Q.T., Wallace, M., Nerbonne, J.M., Lichtman, J.W., and Sanes, J.R. (2000). Imaging neuronal subsets in transgenic mice expressing multiple spectral variants of GFP. Neuron *28*, 41-51.

Galvan, A., and Wichmann, T. (2023). Basal ganglia neurons in healthy and parkinsonian primates generate recurring sequences of spikes. J Neurophysiol *129*, 1010-1020.

Kondo, T., Saito, R., Otaka, M., Yoshino-Saito, K., Yamanaka, A., Yamamori, T., Watakabe, A., Mizukami, H., Schnitzer, M.J., Tanaka, K.F.*, et al.* (2018). Calcium Transient Dynamics of Neural Ensembles in the Primary Motor Cortex of Naturally Behaving Monkeys. Cell Rep *24*, 2191-2195 e2194.

Lestienne, R., and Strehler, B.L. (1987). Time structure and stimulus dependence of precisely replicating patterns present in monkey cortical neuronal spike trains. Brain Res *437*, 214-238.

Masilamoni, G.J., and Smith, Y. (2018). Chronic MPTP administration regimen in monkeys: a model of dopaminergic and non-dopaminergic cell loss in Parkinson's disease. J Neural Transm (Vienna) *125*, 337-363.

McFarland, N.R., and Haber, S.N. (2001). Organization of thalamostriatal terminals from the ventral motor nuclei in the macaque. J Comp Neurol *429*, 321-336.

Middleton, F.A., and Strick, P.L. (2000). Basal ganglia and cerebellar loops: motor and cognitive circuits. Brain Res Brain Res Rev *31*, 236-250.

Nachev, P., Kennard, C., and Husain, M. (2008). Functional role of the supplementary and pre-supplementary motor areas. Nat Rev Neurosci *9*, 856-869.

Oguchi, M., Jiasen, J., Yoshioka, T.W., Tanaka, Y.R., Inoue, K., Takada, M., Kikusui, T., Nomoto, K., and Sakagami, M. (2021). Microendoscopic calcium imaging of the primary visual cortex of behaving macaques. Sci Rep *11*, 17021.

Parker, J.G., Marshall, J.D., Ahanonu, B., Wu, Y.W., Kim, T.H., Grewe, B.F., Zhang, Y., Li, J.Z., Ding, J.B., Ehlers, M.D*., et al.* (2018). Diametric neural ensemble dynamics in parkinsonian and dyskinetic states. Nature *557*, 177-182.

Picard, N., and Strick, P.L. (1996). Motor areas of the medial wall: a review of their location and functional activation. Cereb Cortex *6*, 342-353.

Sheintuch, L., Rubin, A., Brande-Eilat, N., Geva, N., Sadeh, N., Pinchasof, O., and Ziv, Y. (2017). Tracking the Same Neurons across Multiple Days in Ca²⁺ Imaging Data. Cell Reports *21*, 1102-1115.

Strick, P.L., Dum, R.P., and Rathelot, J.A. (2021). The Cortical Motor Areas and the Emergence of Motor Skills: A Neuroanatomical Perspective. Annu Rev Neurosci *44*, 425-447.

Tanji, J., and Mushiake, H. (1996). Comparison of neuronal activity in the supplementary motor area and primary motor cortex. Brain Res Cogn Brain Res *3*, 143-150.

Tarantal, A.F., Noctor, S.C., and Hartigan-O'Connor, D.J. (2022). Nonhuman Primates in Translational Research. Annu Rev Anim Biosci *10*, 441-468.

Vormstein-Schneider, D., Lin, J.D., Pelkey, K.A., Chittajallu, R., Guo, B., Arias-Garcia, M.A., Allaway, K., Sakopoulos, S., Schneider, G., Stevenson, O*., et al.* (2020). Viral manipulation of functionally distinct interneurons in mice, non-human primates and humans. Nat Neurosci.

Yost, O.C., Downey, A., and Ramos, K.S. (2023). Nonhuman Primate Models in Biomedical Research: State of the Science and Future Needs. In Nonhuman Primate Models in Biomedical Research: State of the Science and Future Needs, O.C. Yost, A. Downey, and K.S. Ramos, eds. (Washington (DC)).

Zhou, P., Resendez, S.L., Rodriguez-Romaguera, J., Jimenez, J.C., Neufeld, S.Q., Giovannucci, A., Friedrich, J., Pnevmatikakis, E.A., Stuber, G.D., Hen, R*., et al.* (2018). Efficient and accurate extraction of in vivo calcium signals from microendoscopic video data. Elife *7*.

REAGENT OR RESOURCE	SOURCE	IDENTIFIER
Plasmids		
pAAV TREGCaMP6f	Addgene	Cat # 97410
pAAV ThyStTA	Addgene	Cat # 97411
Viral vectors		
AAV5-TRE-GCAMP6f	Vigene Biosciences	n/a
AAV5-ThyStTA	Vigene Biosciences	n/a
Antibodies		
Chicken anti-GFP (immunofluorescence)	Millipore	Cat # 06-896 RRID: AB_310288
Rabbit anti-GFP (immunoperoxidase)	Thermo Fisher (Invitrogen)	Cat # A-11122 RRID: AB_221569
Mouse anti-MAP2	Millipore	Cat # MAB3418 RRID: AB_11212326
Rabbit anti-GABA	Sigma	Cat # A2052 RRID: AB_477652
Biotinylated goat anti-rabbit	Vector	Cat # BA1000 RRID: AB_2313606
Biotinylated goat anti-mouse	Vector	Cat # BA9200 RRID: AB_2336171
Donkey anti-chicken (Fluorescein)	Jackson Lab	Cat # 703-095-155 RRID:AB_2340356
Donkey anti-rabbit (Rhodamine red-X)	Jackson Lab	Cat # 711-295-152 RRID:AB_2340613

Table 1: Key Resources

Animal ID	Structure	Number of sessions	Total cells identified at least in one session	Cells identified in more than one session
Q	SMA	7	129	23
F	SMA	6	61	17
U	SMA	5	63	15
U	M1	4	37	6
V	M1	2	23	1

Table 2: Number of sessions and cells identified per imaging site.

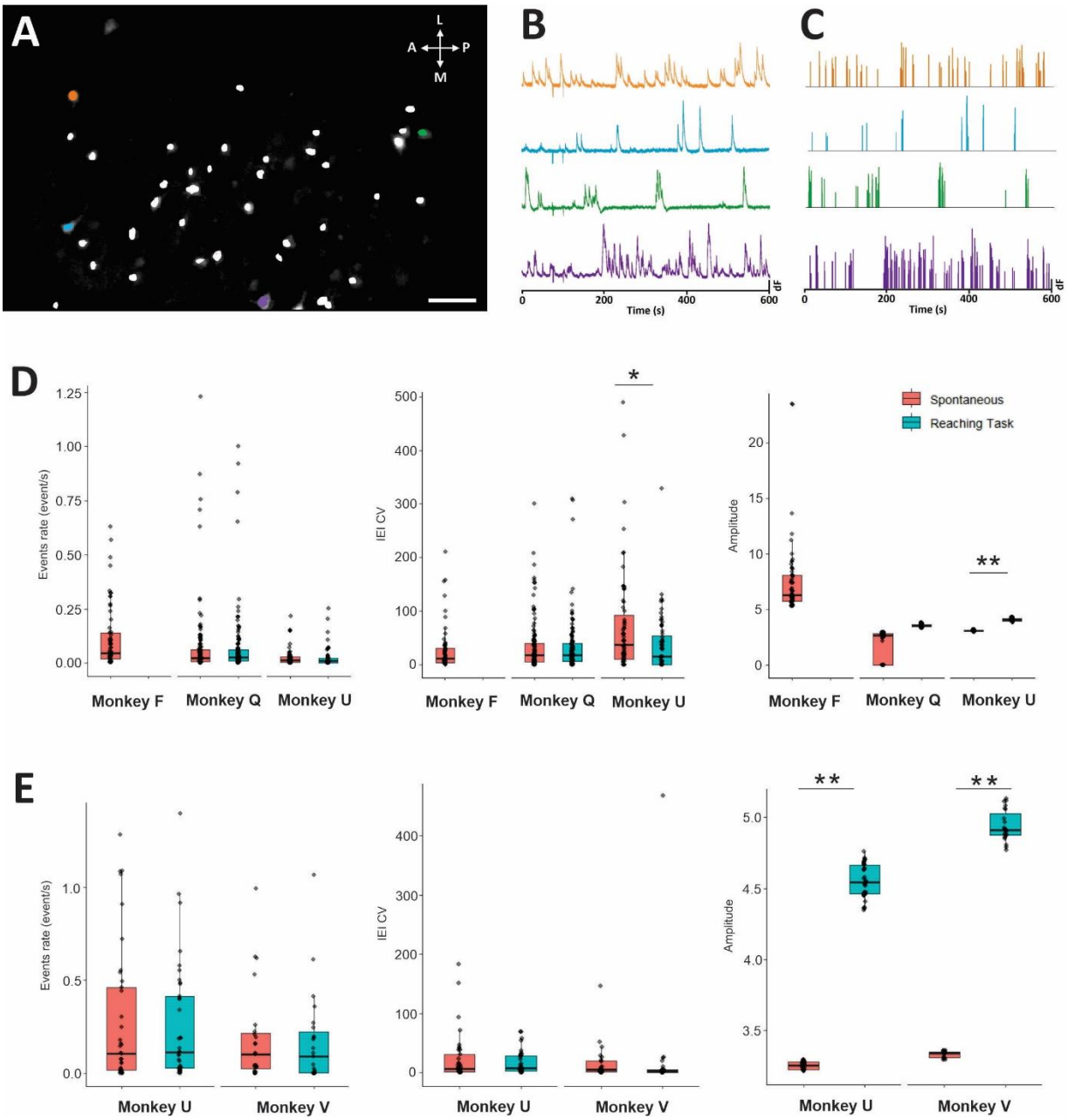

Figure 1: Steps of analysis and general description of cell activity A: Maximal intensity of GCaMP6f fluorescence in the SMA over the course of a single example session (Monkey Q), overlapped with the map of cells (white) extracted using CNMF-E. Orange, blue, green, and purple are example cells shown in B and C. Scale bar: 100 µm. **B:** Raw traces of calcium transients (dF, peak-normalized) during spontaneous activity. **C:** Calcium events detected from the calcium traces in B using the deconvolution method. **D:** Box plots summarizing the event rate (events/s), inter-event interval coefficient of variation (IEI CV) and amplitude of events detected across all sessions in Monkey F, Q and U in the SMA in the spontaneous condition (red) and during the arm reaching task (blue). The horizontal bar in each box indicates the median, each circle indicates the median value for a cell. **E:** Box plots summarizing the event rate (events/s), IEI CV and amplitude of events detected across all sessions in Monkey U and V in M1 in spontaneous (red) and during the reaching task (blue). * $p < 0.05$, ** $p < 0.01$; Wilcoxon sum rank test.

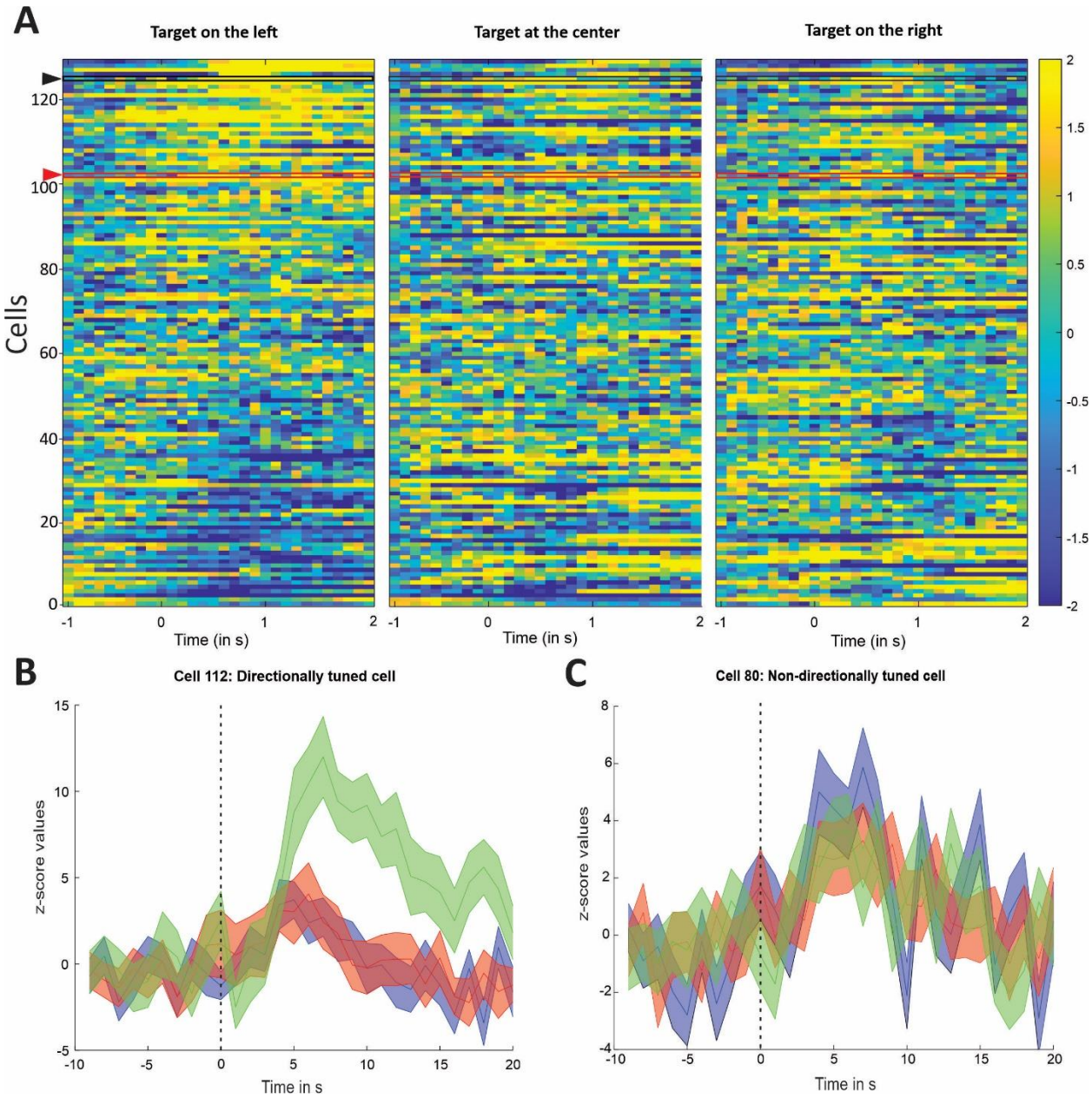

Figure 2: Different responses of SMA cells to target laterality. A: Heat maps of the Z-scored raw calcium traces for each cell in the population, aligned on the appearance of the target at the right, center or left of the screen during the single target reaching task in Monkey Q (n=129 cells, average of 30 trials/conditions). On the left panel, the cells have been sorted on their directional selectivity. On the middle and right panel, cells are sorted in the same order as left panel. The activities of cells #112 and #80 are indicated by the black and red arrow, respectively. **B:** Example of a directionally tuned cell (cell # 112) with a higher significant increase of activity on the presentation of the target on the left. The cell's activity is aligned on the appearance of the target marked by the vertical dash line. Colored curves represent the average Z-score activity ± SD separately for left (green), central (red) and right (blue) targets. **C:** Example of a non-directionally tuned cell (cell #80) which calcium activity significantly increased to the presentation of all targets. Cell activity is aligned on the appearance of the target marked by the vertical dash line. Same legend as panel B.

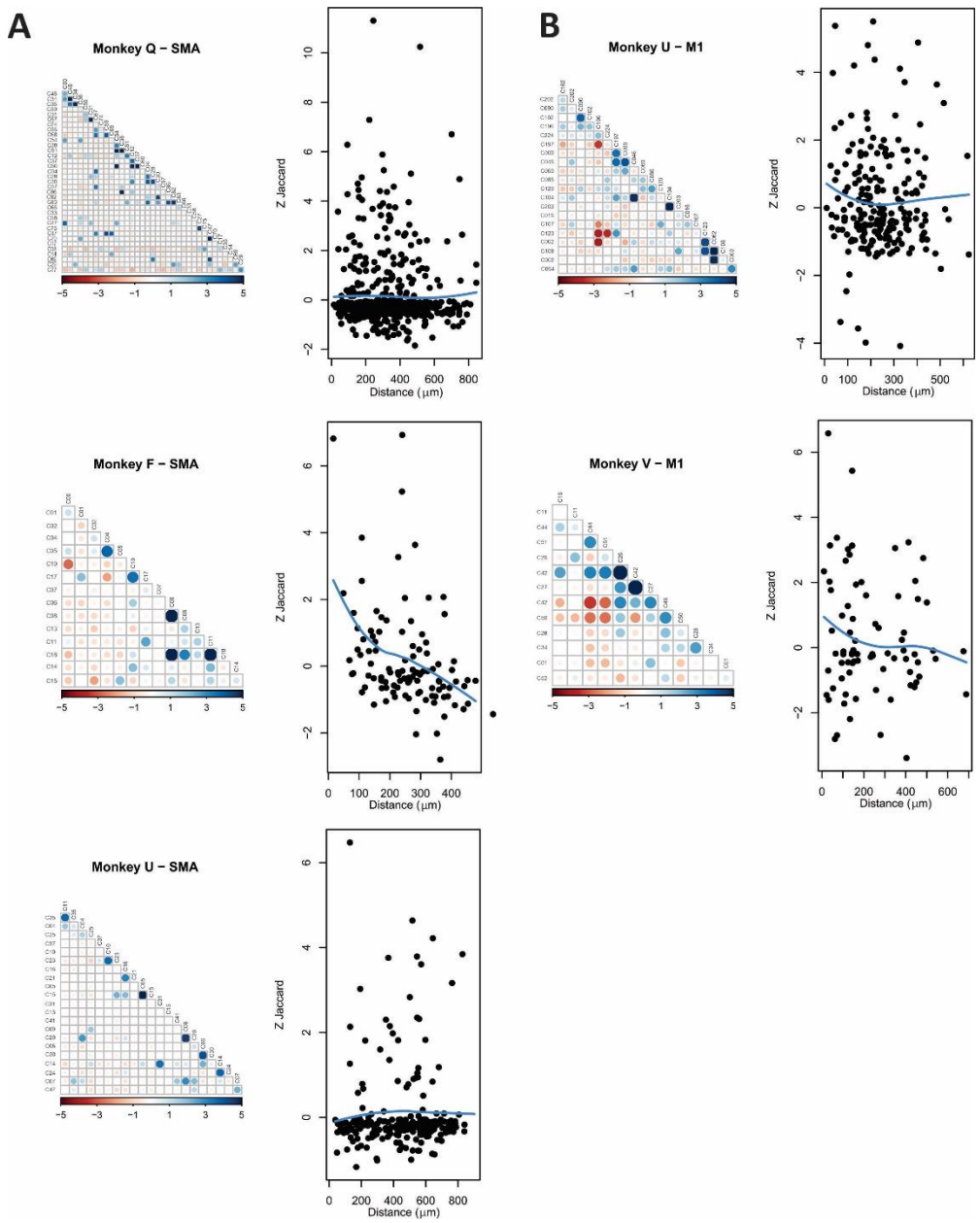

Figure 3: Coactivation between cells events in the spontaneous state in both SMA and M1. A: On the left are the coactivation plots based on recordings during the spontaneous condition in SMA in one example session for Monkeys Q, U and F. Colored dots represent the result of the normalized Jaccard index (Z-Jaccard) for each cell pairing. Large/dark blue circles indicate positive values of Z-Jaccard and large/dark red circles indicate negative values of Z-Jaccard. The right panels represent the correlation plots between Z-Jaccard index and distance between the centroids of the cells, in µm, for each corresponding session shown at the left. **B:** On the left are the coactivation plots based on recording during the spontaneous condition in M1 in one example session for Monkeys U and V. Colored dots represent the result of the normalized Jaccard index (Z-Jaccard) for each cell pairing. Large/dark blue circles indicate positive values of Z-Jaccard and large/dark red circles indicate negative values of Z-Jaccard. The right panels represent the correlation plots between Z-Jaccard index and distance between the centroids of the cells, in µm, for each corresponding session on the left.

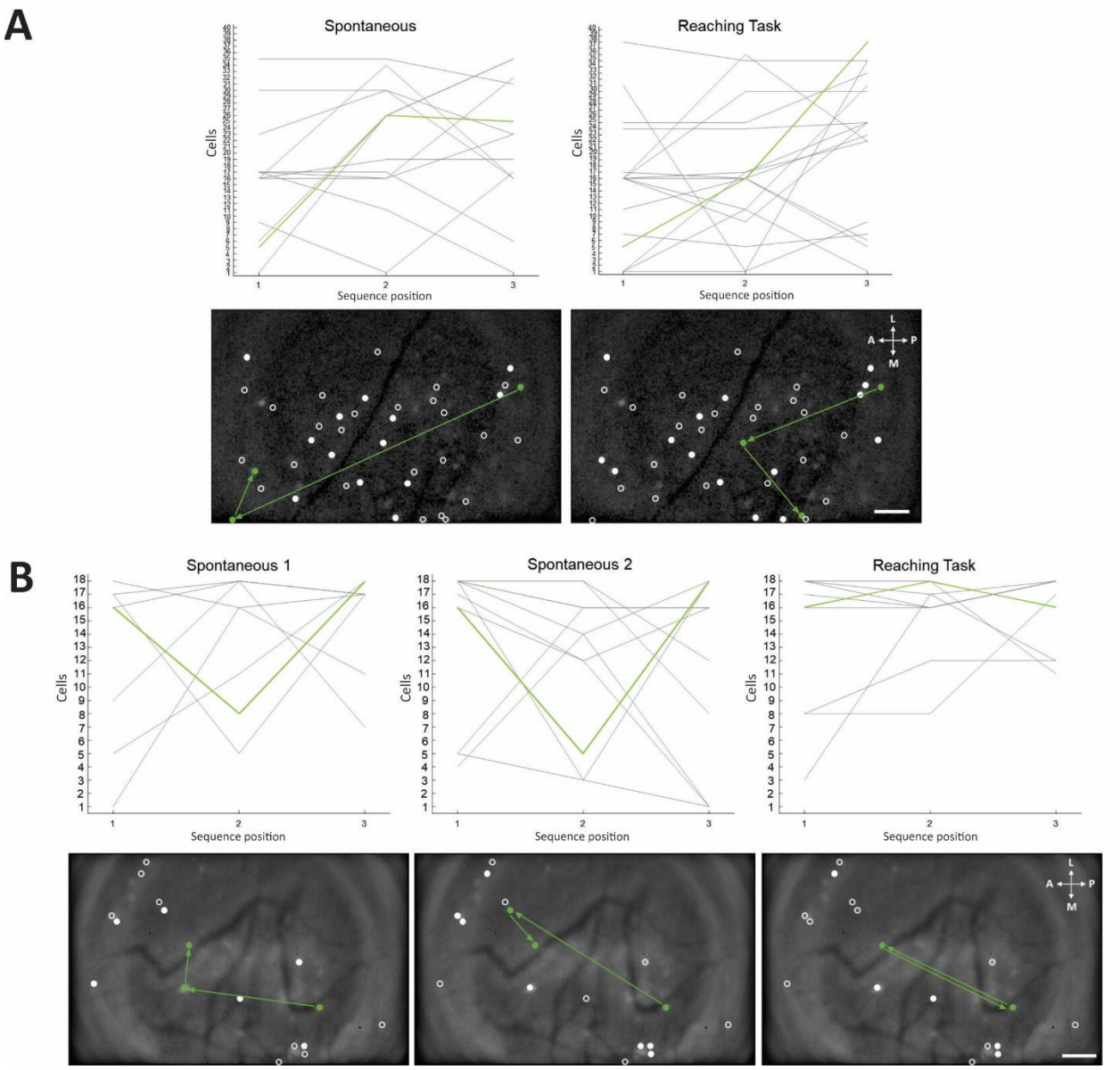

Figure 4: Repeating sequences of calcium events involving several neurons in the spontaneous condition and during the reaching task. A: Top row, the connectograms show all the sequences found across 40 cells in the SMA in an example session for Monkey Q, during spontaneous and reaching task. The x axis indicates the temporal position of the cell within a sequence. An example sequence starting with cell 5 in both conditions is shown in green. Below is the maximal intensity of GCaMP6f fluorescence in the SMA over the same session overlapped with the spatial representation of the example (green arrows) sequences in spontaneous (left) and during the reaching task (right). Cell #5 initiates the sequence, which is followed by different cells in spontaneous and reaching task. The green circles illustrate the three cells involved in the sequence and the green arrows indicate the temporal order. White dots indicate cells involved in other sequences and white circles indicate all the cells detected during the session. **B:** Sequences found across 18 cells in the SMA in an example session for Monkey Q, during two separate 10 minutes recordings in spontaneous (1 and 2) and during the reaching task. Same conventions as described for figure 4A. Scale bar: 100 µm.

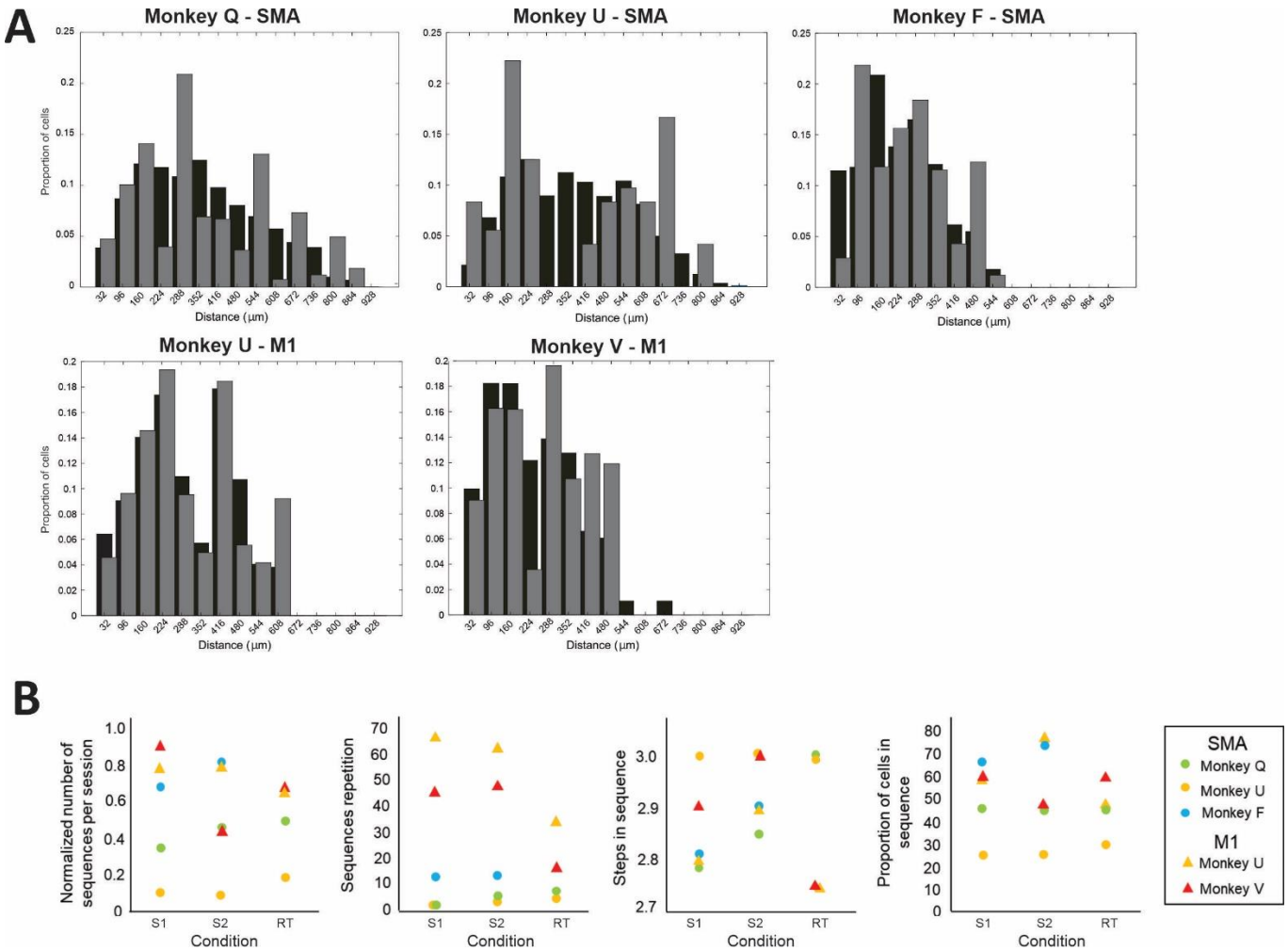

Figure 5: Distribution of cells involved in sequences and sequence parameters A: Black bars indicate the distribution of the centroids of all the cells recorded across all sessions in the spontaneous condition for each monkey in SMA (top) and M1 (bottom). in black. Grey bars indicate the distribution of the centroids of the cells involved in sequences. Note overlap of the distributions, indicating that cells involved in sequences were not clustered, but spread across the field of view. **B:** Parameters of sequence occurrence. The graphs show median values across all the sessions recorded for each monkeys Q (green), U (yellow) F (blue) and V (red) in the SMA (circle) and M1 (triangle). Data is binned in 10 min of recording in spontaneous (S1 and S2) and during the reaching task RT).

SUPPLEMENTARY MATERIAL

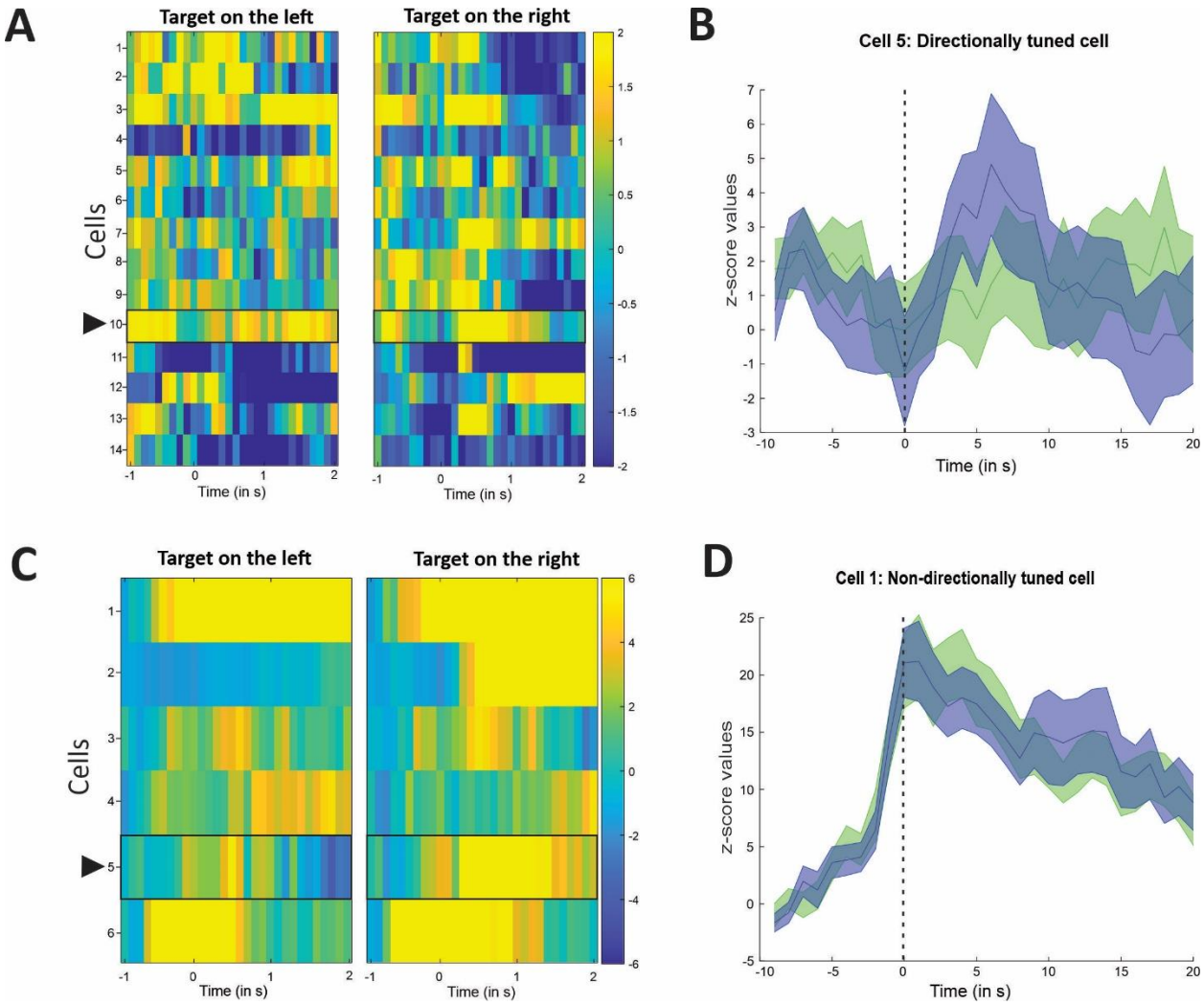

Figure S1: Different responses of SMA and M1 cells to target laterality. A: Heat maps of the Z-scored raw calcium traces of each cell in an example session in SMA, aligned on the appearance of the right or left target during the two-target reaching task in Monkey U (n=14 cells, 62 trials left target, 51 trials right target). On the left panel, the cells have been sorted on their selectivity. On the right panel, cells are sorted in the same order as panel left. The activity of cell #5 is indicated by the black arrow. **B:** Example of directionally tuned cell with a significant increase of activity selectively toward the right target. The activity of cell #5 was aligned on the appearance of the second target marked by the vertical dash line. Colored curves represent the average z-score activity ± SD separately for left (green), and right (blue) targets. **C:** Heat maps of the Z-scored raw calcium traces of each cell in an example session in M1, aligned on the appearance of the right or left target during the two- target reaching task in Monkey U (n=6 cells, 50 trials/condition). On the left panel, the cells have been sorted on their selectivity. On the right panel, cells are sorted in the same order as panel left. The activity of cell #1 is indicated by the black arrow. **E:** Example of non-directionally tuned cell with a significant increase toward both right and left targets. Same legend as panel B.

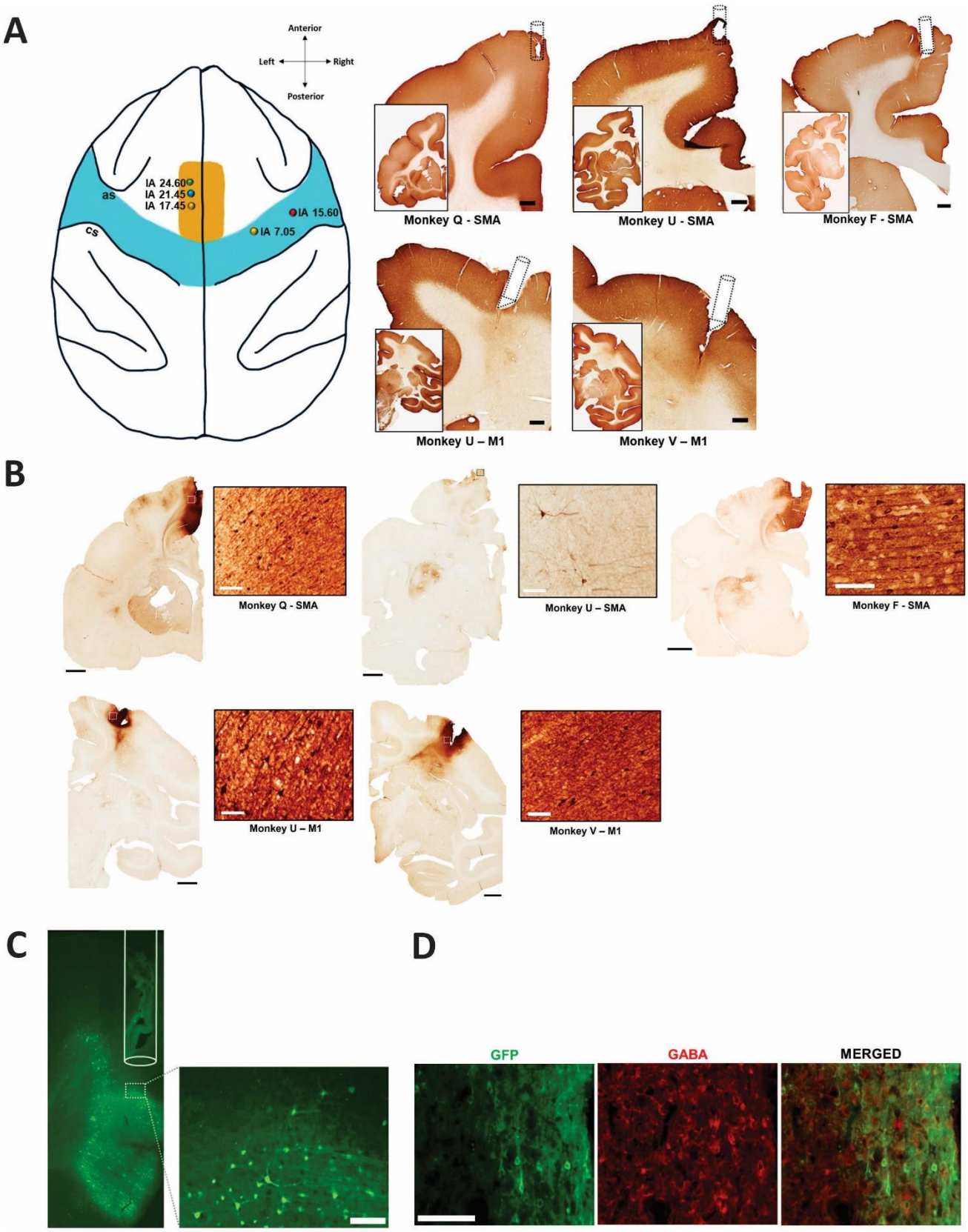
A
Anterior
Left
Right
Posterior
as
cs
IA 24.60
IA 21.45
IA 17.45
IA 15.60
IA 7.05
Monkey Q - SMA
Monkey U - SMA
Monkey F - SMA
Monkey U – M1
Monkey V – M1
B
Monkey Q - SMA
Monkey U – SMA
Monkey F - SMA
Monkey U – M1
Monkey V – M1
C
D
GFP
GABA
MERGED

Figure S2: Assessment of GCaMP6f expression and lens location in the SMA and M1. A: At left, illustration indicating the location of the lenses in the SMA (orange area) for monkey Q (orange dot), F (blue dot) and U (yellow dot) with the corresponding interaural coordinate (based on the atlas by Paxinos et al 2000), in the left hemisphere. The location and interaural coordinates of the prisms in M1 (blue area) are illustrated for monkey U (yellow dot) and V (red dot). as, arcuate sulcus, cs, central sulcus. At the right, MAP-2 stained brain sections show reconstrucitons of the lens placement in the SMA (top row) and prism placement in M1 (bottom row). Black scale bar, 1 mm. **B:** Expression of GCaMP6f (revealed with GFP immunoperoxidase) at the level of the SMA in the left hemisphere (monkeys Q, U and F), and M1 in the right hemisphere (monkeys U and V). The white rectangles are shown at higher magnification at the right. Black scale bar, 4 mm. White scale bar, 100 µm. **C:** Endogenous green fluorescence of GCaMP6f expression in a serial section of A and B for monkey Q, left hemisphere. Reconstruction of lens placement (white line), lens diameter is 1 mm. The white rectanlge is shown at higher higher magnification on the right. White scale bar, 100 µm. **D:** Double immunofluorescence for GFP and GABA. First panel shows GFP (GCaMP6f-positive) cellsin M1 (monkey U, green), second panel shows GABA-positive (red) cells in the same section. Last panel (merged) shows lack of cells co-expressing both GCaMP6f and GABA (merged) indicating that GCaMp6f expressing cells are not GABAergic interneurons. White scale bar, 100 µm.